Primljen / Received: 22.1.2025.
Ispravljen / Corrected: 3.6.2025.
Prihvaćen / Accepted: 25.6.2025.
Dostupno online / Available online: 10.7.2025.

Ductility of reinforced concrete walls with composite cross-sections

Authors:

Hrvoje Čagalj, MCE
EKONERG d.o.o.
cagalj1992@gmail.com
Corresponding author

Prof. **Tomislav Kišiček**, PhD. CE
University of Zagreb
Faculty of Civil Engineering
tomislav.kisicek@grad.unizg.hr

Assoc.Prof. **Mario Uroš**, PhD. CE
University of Zagreb
Faculty of Civil Engineering
mario.uros@grad.unizg.hr

Research Paper

Hrvoje Čagalj, Tomislav Kišiček, Mario Uroš

Ductility of reinforced concrete walls with composite cross-sections

The EN 1998-1 standard does not provide direct expressions for the ductility control of reinforced concrete walls with composite cross-sections, which complicates their design and dimensioning. In this paper, the ductility of walls with C- and T-shaped cross-sections was analyzed using SAP2000 v24.0.0. The effects of the dimensionless longitudinal force coefficient, flange confinement, the amount of compressive and tensile reinforcement, and the direction of the moment of resistance of the section were investigated. The negative impact of increasing tensile reinforcement and longitudinal force was highlighted, while confinement and increased compressive reinforcement were found to improve ductility. The maximum allowable relative compressive strain of concrete and the height of the compression zone within the cross-section were identified as key factors controlling the available ductility of the section.

Key words:
reinforced concrete, walls with composite cross-sections, ductility, elasto-plastic response, plastic hinge, confined concrete

Prethodno priopćenje

Hrvoje Čagalj, Tomislav Kišiček, Mario Uroš

Duktilnost armiranobetonskih zidova složenih poprečnih presjeka

Norma EN 1998-1 ne daje izravne izraze za kontrolu duktilnosti armiranobetonskih zidova složenih poprečnih presjeka, što otežava njihovo oblikovanje i dimenzioniranje. U ovome radu analizirana je duktilnost zidova s poprečnim presjecima C i T primjenom SAP2000 v24.0.0. Istraženi su utjecaji bezdimenzijskoga koeficijenta uzdužne sile, ovijanja pojasnica, količine tlačne i vlačne armature te smjera momenta nosivosti presjeka. Istaknut je negativan utjecaj povećanja vlačne armature i uzdužne sile, dok ovijanje i povećanje tlačne armature poboljšavaju duktilnost. Kao ključni faktori koji kontroliraju raspoloživu duktilnost presjeka identificirani su maksimalna dopuštena relativna tlačna deformacija betona i visina tlačnog područja poprečnog presjeka.

Ključne riječi:
armirani beton, zidovi složenoga poprečnog presjeka, duktilnost, elastoplastični odziv, plastični zglob, ovijeni beton

1. Introduction

As part of the Mediterranean–Trans-Asian seismic belt, almost the entire territory of the Republic of Croatia is characterized by significant seismic activity. This is especially true for the coastal region and the northwestern part of the country, with southern Dalmatia being particularly affected. Earthquakes in Croatia occur as a result of the interaction and accumulation of tectonic stresses caused by the subduction of the Adriatic microplate (Adria) beneath the European lithosphere in the convergent boundary zone between the African and Eurasian plates (in the coastal area, the Dinarides, extending to the southwestern part of the Pannonian Basin), or as a result of deformation within larger tectonic units (e.g., in the interior of Croatia or the central Adriatic) [1].

An earthquake, as an action on a structure, differs significantly from other types of loads and therefore requires a specific approach by designers when shaping and dimensioning structures. Some specific characteristics of seismic action include:

- uncertainties in the estimation of the relevant action parameter, namely the peak ground acceleration
- short duration of the earthquake
- high intensity
- irregular occurrence
- It causes extensive damage to the affected area; the Zagreb earthquake caused 11.301 billion euros in damage in just 10 seconds [2].

The approach to designing structures for static loads is based on the expression:

$$\frac{[R_k]}{\gamma_m} \geq \gamma_f \cdot [E_k] \quad (1)$$

where:

R_k - structural resistance
E_k - load on the structure
γ_f & γ_m - partial factors for loads and materials,

which ensures that if the structural resistance R_k is greater than the action E_k, considering the partial safety factors, the structure can be considered safe. This approach is straightforward, based on forces, and clearly illustrates the safety margin as the ratio of resistance to action. Figure 1a) illustrates the concept of verifying structural capacity according to expression (1). The difference between static loads and seismic loads lies in the limited duration of the earthquake and the change in the sign of the structure's displacements during seismic action, whereas static loads have a constant direction and magnitude over time. It is important to note that when ductile structures reach the plastic hinge formation under static loads, due to the constant direction and magnitude of the load, accelerated deformation and structural failure occur. However, when plastic hinges form under seismic loading, because of the limited duration of ground shaking and the reversal of deformation directions (vibrations), accelerated deformation in one direction and exhaustion of structural capacity do not occur. Therefore, seismic action is better considered in terms of the energy that the structure absorbs during the earthquake duration, which must be dissipated through available mechanisms. Verification of structural capacity under seismic action is performed according to the expression:

$$\frac{\left[W^u_{supply}\right]}{\gamma_m} \geq \gamma_W \cdot \left[W_{demand}\right] \quad (2)$$

where:

γ_m & γ_W -partial factors for material and energy absorption
$[W^u_{supply}]$ - strain energy
$[W_{demand}]$ - kinetic energy induced in the structure during vibration.

Figure 1.b shows the concept of safety verification for seismic actions according to expression (2) which is based on comparing the amount of energy absorbed during the earthquake duration and the energy the structure can dissipate. The absorbed energy is equal to the area under the force–displacement curve for the required or imposed displacement of the structure. The amount of energy the structure can dissipate is defined as the area under the force–displacement curve for the maximum available displacement of the structure.

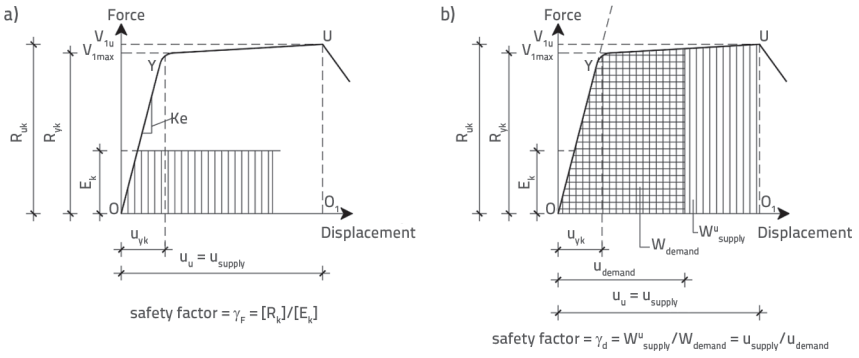

Figure 1. Concept of safety verification: a) static loads; b) seismic action (where $\gamma_{F\,i}$ γ_d partial coefficients of the building for static and earthquake actions)

2. Dissipation of seismic energy and system ductility

From the previous chapter, the importance of the structure's ability to deform in the inelastic range and dissipate the induced energy during seismic action is evident. The difference in response between an elastic system and an inelastic system is illustrated using the example of two single-degree-of-freedom systems with equal mass and stiffness, freely oscillating and having the same velocity when passing through the initial equilibrium position. Figures 2 and 3 show qualitative relationships between force and displacement. The areas under the force–displacement curves represent the work done by the force on the displacement, i.e., the change in the system's energy. The first system exhibits elastic behavior

with resistance V1, while the second system exhibits elasto-plastic behavior with resistance V_2, where $V_2 < V_1$.

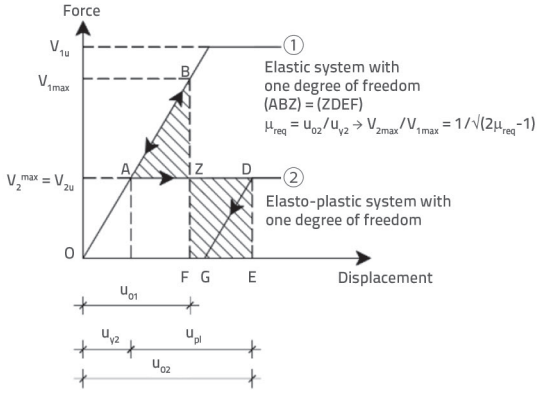

Figure 2. Quantitative relationship of the response of a single-degree-of-freedom system to seismic action [3,4]

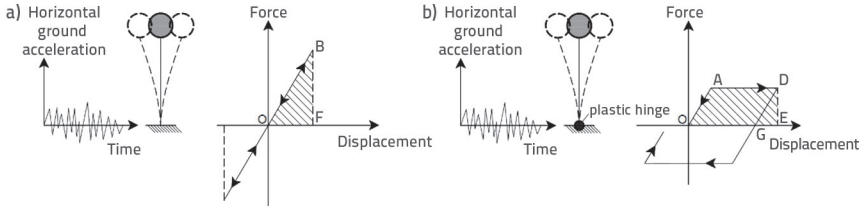

Figure 3. Response of a single-degree-of-freedom system, a) elastic response; b) elasto-plastic response [3,4]

The first system's displacement from the equilibrium position by u_{o1} corresponds to the development of strain energy, which is equal to the area of triangle OBF and also equal to the kinetic energy:

$$\frac{1}{2}Mv_{max}^2 = \frac{1}{2}Ku_{01}^2 \tag{3}$$

The second system, since $V_2 < V_1$ cannot develop an elastic response up to the level V_1 like the first system, instead, at the force level V_2 it begins to yield and behaves elasto-plastic, forming a plastic hinge at the base and reaching a displacement u_{o2}. The area OADE represents the potential energy of the system at the moment it reaches the maximum displacement u_{o2}, which is equal to the kinetic energy at the moment the system passes through the equilibrium position, i.e., at maximum velocity. After reaching the maximum displacement u_{o2} the system begins to return to the initial position under the action of force V_2, at the moment when $V_2 = 0$, the system's potential energy has been converted into kinetic energy equal to the area of triangle EDG. The remaining energy, equal to the area OADG, is dissipated in the plastic hinge region by being converted into irreversible forms of energy.

From the above, it follows that in elastic systems without damping, there is a continuous exchange between kinetic and potential energy, thus preserving the total amount of energy. In elasto-plastic systems, only a portion of the kinetic energy is converted into potential energy from cycle to cycle due to the presence of damping, and the total amount of energy dissipated per cycle depends on the value of u_{pl}. Therefore, it can be concluded that a structure can resist seismic action in two basic ways.

The first way is by developing high resistance V_1 within the elastic range. The second way is by developing significantly lower resistance V_2 and utilizing the capacity for plastic deformation up to the amount u_{pl}. The ability of a structure to undergo plastic deformation is called ductility, and as will be shown, it is of crucial importance for earthquake-resistant structures. Ductility factors in general form are defined as ratios of some quantity at failure to that at the onset of yielding of the tensile reinforcement. Three ductility factors are distinguished: displacement ductility factor – $\mu_{\varnothing}$, element rotation ductility factor – $\mu_{\varnothing}$, and cross-section curvature ductility factor– $\mu_{\varnothing}$. [3, 4].

To achieve a high level of resistance V_1, the entire system must be designed along its height for significantly higher forces compared to an elasto-plastic system that attains resistance level V_2, and develops a plastic hinge at its base, allowing for the system's ductility and a value of plastic deformation u_{pl}. Since plastification is localized, it is economically advantageous to design structures with predefined plastic hinge regions that require additional reinforcement, ensuring sufficient ductility capacity compared to the significantly greater amount of reinforcement that would be needed throughout the entire height of the system if an elastic response were required.

Besides the mentioned reinforcement savings, according to [5] by selecting a higher reduction of seismic forces, the demand on the bearing capacity of the foundation soil decreases, the structure possesses greater resistance to earthquakes stronger than those anticipated, it is less sensitive to uncertainties in defining seismic actions, and the accelerations of the structure are limited by reducing the ordinate of the design spectrum. This, in turn, reduces damage to non-structural elements sensitive to accelerations, such as out-of-plane failures of partition walls. The described reduction of seismic forces, from, V_1V_2, is carried out according to the current standard HRN EN 1998-1 [6] by selecting an appropriate behavior factor, which depends on the ductility class, type of structural system, and regularity of the system in height. The type of structural system and its regularity are often determined by the building's purpose and design, while the choice of ductility class is left to the designer – the structural engineer. HRN EN 1998-1 [6] defines three ductility classes, DCL – low ductility class, DCM – medium ductility class and DCH – high ductility class.

The relationship between the chosen behavior factor and the required ductility of the structure according to HRN EN 1998-1 [6] is given by the relation between the curvature ductility factor in the plastic hinge region and the basic value of the behavior factor q_0:

$$\begin{aligned} \mu_\phi &= 2\cdot q_0 - 1 \quad \text{if} \quad T_1 \geq T_C \\ \mu_\phi &= 1 + (2\cdot q_0 - 1)\, T_1/T_C \quad \text{if} \quad T_1 < T_C \end{aligned} \tag{4}$$

where:

μ_ϕ - The ratio of the post-yield curvature at 85 % of the ultimate moment capacity to the curvature at the yielding of the tensile reinforcement

T_c - upper limit of the period with the branch of constant spectral acceleration

T_1 - fundamental vibration period of the building in lateral motion and the considered direction.

Furthermore, in critical regions of primary seismic elements with longitudinal reinforcement made of steel grade B, the ductility factor with respect to curvature μ_ϕ should be at least 1,5 times greater than the value specified in expressions (4). From this, it is evident that the required ductility factor with respect to curvature exceeds the basic value of the behavior factor.

To achieve the required ductility of critical regions, i.e., curvature of the cross-section, the greatest deformation demand is placed on the fibers farthest from the neutral axis, whether tensile or compressive. Reinforcing steel grades B500B and B500C have a yield strength of f_{yk} = 500MPa, tensile and compressive strain at yield equal to: $\varepsilon_s = f_{yd}/E_s$ = 2,174 ‰, and ultimate strain equal to 50 ‰ for grade B and 75 ‰ for grade C. The ratio of tensile strength to yield strength of reinforcement for grade B is $(f_t/f_y)_k \geq 1{,}08$, and for grade C it is $1{,}15 \leq (f_t/f_y)_k \leq 1{,}35$. For concrete classes lower than < C50/60 the value of compressive strain at yield is ε_{c2} = 2 ‰ for the design parabola-rectangle diagram, and ε_{c3} = 1,75 ‰ for the bilinear design diagram. The ultimate strain for both diagrams is 3,5 ‰. The ratio of strains at yield and ultimate is considerably less favorable for concrete compared to reinforcing steel, which becomes especially significant in cross-sections with larger compressive forces where the neutral axis is farther from the most compressed fibers. For the same curvature, this results in a greater deformation demand on the edge regions.

3. Confined concrete

The presence of compressive stresses σ_2 and σ_3, where $\sigma_2 \approx \sigma_3$, along with the principal compressive stress σ_1 which is relatively large compared to σ_2 and σ_3, shows beneficial effects on the concrete stress–strain diagram, primarily by increasing the ultimate strain. Sources of triaxial compressive stress states in concrete structures may vary: beam-column joints, column-foundation connections, installation of closely spaced closed stirrups in elements, and confinement of the element using FRP wraps [5].

It is important to note that Poisson's ratio for concrete is approximately 0,2 for compressive stress levels less than < 0,95· f_c, where f_c is the compressive strength of concrete. For higher stress levels, it increases up to 0,4 at the ultimate state of concrete, which significantly enhances the effectiveness of confinement, as the increased lateral deformations at failure strongly activate the transverse reinforcement in critical regions [5]. The ratio of lateral compressive stresses σ_2 / σ_3 is of great importance, since in the case of unequal lateral stresses, where $\sigma_2 > \sigma_3$ the equivalent lateral pressure is calculated according to the following expression:

$$(\sigma_2 + 4\sigma_3)/5 \tag{5}$$

which demonstrates the considerable effect of the smaller stress componenta σ_3 [5].

HRN EN 1992-1-1 [7] and HRN EN 1998-3 [8] propose different expressions for the characteristic compressive strength of confined concrete. The expression adopted in HRN EN 1992-1-1 [7] is recommended for the design of new structures and provides somewhat more conservative values compared to the expression from HRN EN 1998-3 [8] which gives more accurate results and is therefore recommended when aiming to precisely model the condition of existing structures.

According to HRN EN 1998-1 [6], sufficient ductility of the cross-section in new reinforced concrete rectangular walls is achieved by installing additional confinement reinforcement in the form of closed stirrups and/or additional reinforcement in "C" and "S" shapes in the critical regions of the walls. The installation of the described reinforcement improves the effectiveness of confinement of the concrete section, denoted as, α, as well as increases the mechanical volumetric reinforcement ratio of the confining reinforcement, ω_{wd}. The verification of sufficient ductility of rectangular wall cross-sections is performed using expression (6):

$$\alpha \cdot \omega_{wd} \geq 30\mu_\phi (\nu_d + \omega_d)\varepsilon_{sy,d}\frac{b_c}{b_0} - 0{,}035 \tag{6}$$

where

α - confinement effectiveness factor

ω_{wd} - mechanical volumetric ratio of confining reinforcement

ν_d - axial load in the seismic design situation, normalized by $A_c f_{cd}$

ω_v - mechanical reinforcement ratio of the boundary element with vertical reinforcement

$\varepsilon_{sy,d}$ - design value of steel strain at yielding

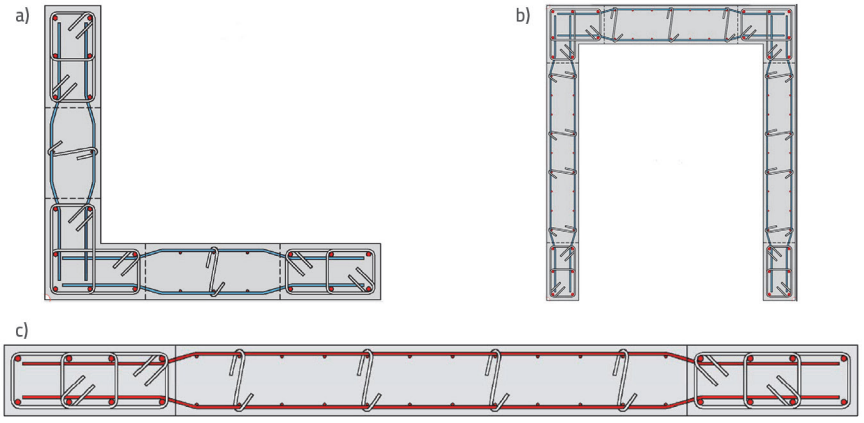

Figure 4. Reinforcement layout of a) "L"-shaped wall, b) "U", "C"-shaped wall, c) rectangular wall [9]

b_c - wall thickness
b_0 - width of the confined core of the column or boundary element of the wall (measured to the centerline of the links/stirrups).

Apart from rectangular walls, Figure 4.c, walls with composite cross-sections-such as walls with end flanges or walls composed of multiple rectangular segments (T-, L-, I-, U-shaped cross-sections, etc.) are commonly used. One typical example of such walls in engineering practice is the core walls of staircases and elevator shafts in buildings, Figure 4.a and 4.b. According to HRN EN 1998-1 [6] for these types of walls, the verification of sufficient cross-sectional ductility is carried out:

a) according to the expression for rectangular cross-sections if the depth of the neutral axis at maximum curvature x_u does not exceed the height of the flange or web
b) if x_u exceeds the height of the flange or web, then according to [5] there are three options:
   - increase the height of the flange so that it is greater than x_u
   - use the general verification method, based on relationships where the curvature ductility factor μ_ϕ is defined as:

$$\mu_\phi = \phi/\phi_y \quad (7)$$

By calculating the curvature at failure of the cross-section–ϕ_u and the curvature at the onset of yielding of the tensile reinforcement–ϕ_y as:

$$\mu_u = \varepsilon^*_{cu}/x_{cu} \quad (8)$$

$$\phi_y = \varepsilon_y/(d-x_y) \quad (9)$$

where:
ϕ_u - curvature at ultimate failure of the cross-section
ϕ_y - curvature at the onset of yielding of the tensile reinforcement
ε^*_{cu} - strain of the most highly compressed fiber of confined concrete
x_{cu} - depth of the neutral axis at maximum curvature for concrete failure
ε_y - strain of steel at yielding
x_y - depth of the neutral axis at the onset of tensile steel yielding
d - effective depth of the cross-section
Estimating the heights of the neutral axes x_u and x_y from the cross-section equilibrium and using the expressions for confined concrete.

Verification is possible using iterative procedures with software solutions. The confinement reinforcement is calculated for the compression flange of width b_c and for the corresponding parts of the web of the cross-section.

   - The third option is to provide confinement of the webs instead of the flanges, which makes sense only if the flanges are not significantly wider than the webs and if the compression zone x_u is relatively small.

As stated, HRN EN 1998-1 [6] does not provide explicit formulas for checking the ductility of walls with composite cross-sections due to the large number of variables involved, and often it is not possible to apply the expressions for rectangular walls (6), so, it is necessary to verify the ductility of such cross-sections according to expressions (7), (8) and (9) using iterative software solutions.

4. Determination of the moment–curvature diagram of cross-sections

The moment–curvature diagram of cross-sections, shown in Figure 5, graphically represents the relationship between the bending moment M, of the section and the curvature ϕ of the section. The curvature of the section is defined as the angle:

$$\phi = (\varepsilon_c+\varepsilon_s)/d \quad (10)$$

where:
ε_c - compressive strain of concrete
ε_s - tensile strain of reinforcement
d - effective depth.

The diagram has three characteristic points. Point 1 represents the state of the cross-section at the appearance of the first crack, i.e., when the tensile strength of the concrete in the most stressed fiber of the cross-section in tension is reached. The expressions for determination are based on a linear distribution of strains over the height of the cross-section and the elastic behavior of the materials. Point 2 represents the state of the cross-section at the occurrence of the first yielding of the reinforcement in tension. Point 3 represents the state of the cross-section at reaching failure, i.e., when the compressive strains of the concrete are exceeded, tensile failure of the reinforcement occurs, or the moment capacity of the cross-section falls to $0{,}85M_{max}$ [10].

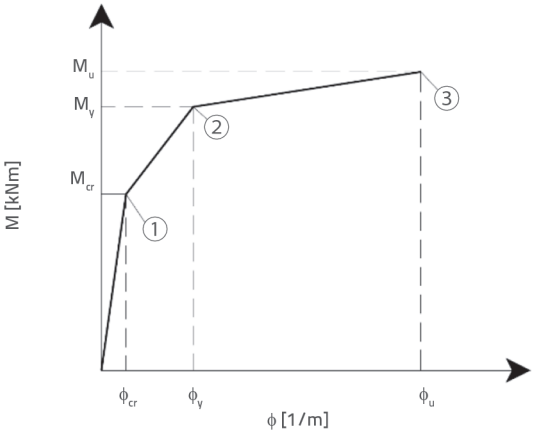

Figure 5. M – ϕ diagram, piecewise linear [10]

5. Analysis of composite reinforced concrete cross sections

To demonstrate the influence of various factors on the final value of the ductility coefficient with respect to the curvature of the cross-section, an analysis was performed on two types of cross-sections: a "T" cross-section and a "C" cross-section. The sections were analyzed for different levels of normalized axial force, ν = 0,20, ν = 0,25, ν = 0,30, ν = 0,35 and ν = 0,40, varying the amount of tensile reinforcement, compressive reinforcement, direction of the bending moment of the section, and the confinement effectiveness of the confined part of the section. The analyzed cross-sections have the following dimensions:

- The "T" cross-section consists of a web 25 cm wide and a flange 25 cm wide and 100 cm, long, with a total height of 250 cm.
- The "C" cross-section consists of a flange 25 cm wide and 200 cm long, a web 25 cm wide, with a total height of 275 cm.

Section 1 is the reference "T" cross-section. In Sections 2 to 5, the tensile reinforcement was increased, while in Sections 6 and 7, the compressive reinforcement was increased. Section 11 is identical to Section 4 but analyzed for the opposite bending moment direction and serves as a reference section for analyzing the effect of confinement of part of the section together with Sections 12 to 15. Section 21 is the reference "C" cross-section. In Sections 22, 23, and 24, the total reinforcement of the section increased. Section 24 serves as a reference section for analyzing the effect of confinement of part of the section together with Sections 31 to 34. The following shows the analyzed cross-sections, with the vector of the axial force and the direction of the bending moment about the major axis displayed in the developed cross-section Figure 6.

For the "T" cross-section, the confinement of the edge region of the web was considered, while for the "C" cross-section, the confinement of the flange was considered. In Figures 6e and 6d the confinement reinforcement is shown only in the compression flange since the change of bending moment sign was not considered. A tabular description of the cross-sections is given in, Table 1:

5.1. Reinforcement steel

For the section analysis, a bilinear design diagram for B500B steel was used. The maximum ultimate strain is 50 ‰, the yield strain is 2,174 ‰, the stress at yield is 434,78 MPa, and the Young's modulus is E = 200000 MPa.

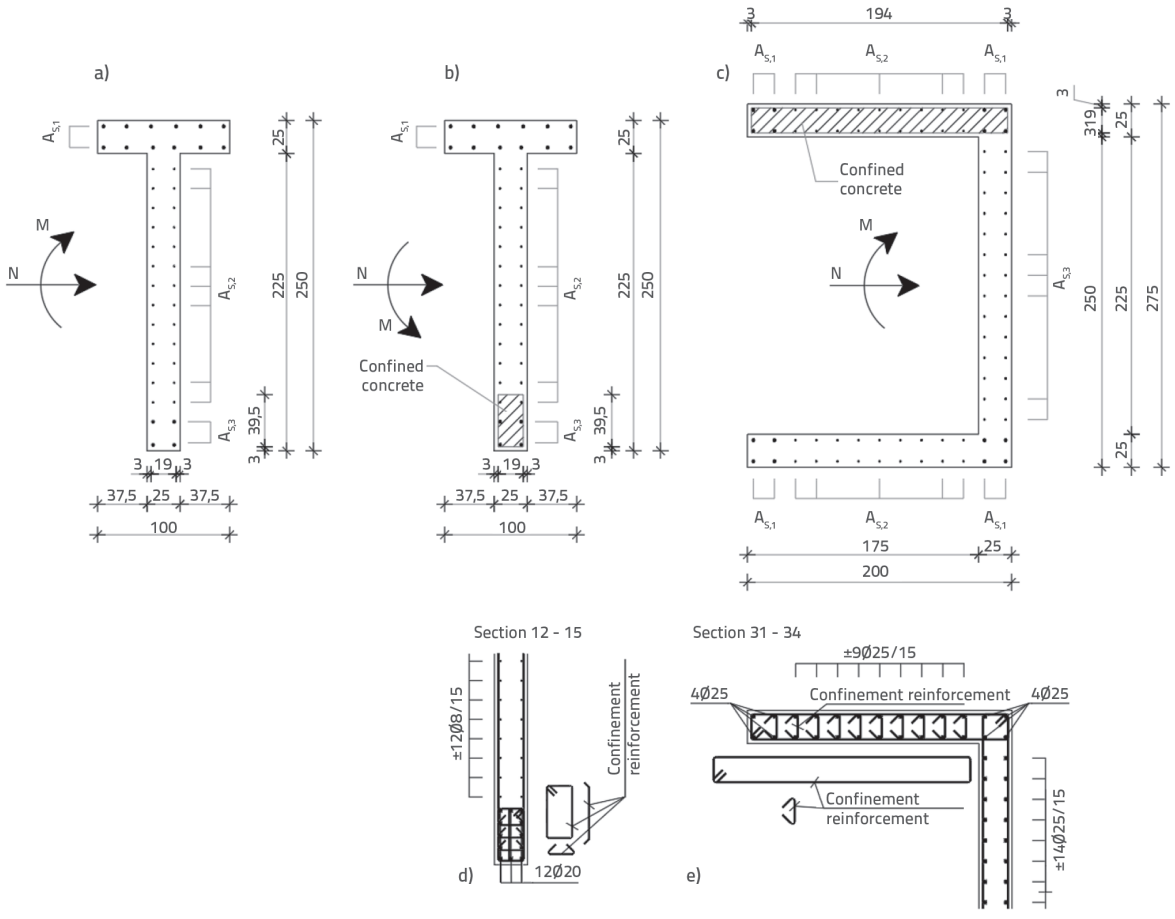

Figure 6. Analyzed cross-sections, a) Cross-section 1 to 11, b) Cross-section 12 to 15 , c) Cross-section 21 to 34, d) reinforcement detail for confinement of Cross-section 12 to 15, e) reinforcement detail for confinement of Cross-section 31 to 34

Table 1. Tabular description of the cross-sections

Section	Section shape	$A_{s.1}$ [cm²]	$A_{s.2}$ [cm²]	$A_{s.3}$ [cm²]	$\alpha\omega_{wd}$
Section 1	T	12Ø16 = 24.12	±13Ø8/15 cm = 13.07	4Ø16 = 8.04	0.00
Section 2	T	12Ø16 = 24.12	±13Ø8/15 cm = 13.07	8Ø16 = 16.08	0.00
Section 3	T	12Ø16 = 24.12	±13Ø8/15 cm = 13.07	8Ø20 = 25.13	0.00
Section 4	T	12Ø16 = 24.12	±12Ø8/15 cm = 12.06	12Ø20 = 37.7	0.00
Section 5	T	12Ø16 = 24.12	±12Ø8/15 cm = 12.06	12Ø25 = 58.90	0.00
Section 6	T	12Ø20 = 37.70	±13Ø8/15 cm = 13.07	4Ø16 = 8.04	0.00
Section 7	T	12Ø25 = 58.90	±13Ø8/15 cm = 13.07	4Ø16 = 8.04	0.00
Section 11	T	12Ø16 = 24.12	±12Ø8/15 cm = 12.06	12Ø20 = 37.7	0.00
Section 12	T	12Ø16 = 24.12	±12Ø8/15 cm = 12.06	12Ø20 = 37.7	0.03640
Section 13	T	12Ø16 = 24.12	±12Ø8/15 cm = 12.06	12Ø20 = 37.7	0.05759
Section 14	T	12Ø16 = 24.12	±12Ø8/15 cm = 12.06	12Ø20 = 37.7	0.11379
Section 15	T	12Ø16 = 24.12	±12Ø8/15 cm = 12.06	12Ø20 = 37.7	0.17153
Section 21	C	4Ø16 = 8.04	±9Ø12/15 cm = 20.36	±14Ø12/15 cm = 31.67	0.00
Section 22	C	4Ø16 = 8.04	±9Ø16/15 cm = 36.19	±14Ø16/15 cm = 56.30	0.00
Section 23	C	4Ø20 = 12.57	±9Ø20/15 cm = 56.55	±14Ø202/15 cm = 87.96	0.00
Section 24	C	4Ø25 = 19.63	±9Ø25/15 cm = 83.36	±14Ø25/15 cm = 137.44	0.00
Section 31	C	4Ø25 = 19.63	±9Ø25/15 cm = 83.36	±14Ø25/15 cm = 137.44	0.01732
Section 32	C	4Ø25 = 19.63	±9Ø25/15 cm = 83.36	±14Ø25/15 cm = 137.44	0.02736
Section 33	C	4Ø25 = 19.63	±9Ø25/15 cm = 83.36	±14Ø25/15 cm = 137.44	0.05163
Section 34	C	4Ø25 = 19.63	±9Ø25/15 cm = 83.36	±14Ø25/15 cm = 137.44	0.07601

5.2. Concrete

For the section analysis, C30/37 concrete was used, with properties from the bilinear design diagram. The design compressive strength of the concrete cylinder is $f_{cd} = f_{ck}/\gamma_C = 30/1{,}5 = 20$ MPa, where f_{ck} is the characteristic 28-day compressive strength and γ_C is the partial factor for concrete. The strain at maximum compressive stress f_c is $\varepsilon_{c3} = 1{,}75$ ‰, and the ultimate compressive strain at failure is $\varepsilon_{cu3} = 3{,}5$ ‰. The characteristic points of the confined concrete diagram were calculated according to HRN EN 1992-1-1 [7] depending on the confinement effectiveness factor α and the mechanical volumetric ratio of the confining reinforcement ω_w. The design lateral compressive stress σ_2 was calculated according to [5] using the expression:

$$\sigma_2 = 0{,}5\alpha\omega_w f_{ck} \tag{11}$$

where:

α - confinement effectiveness factor
ω_w - mechanical volumetric ratio of confining reinforcement
f_{ck} - characteristic 28-day compressive strength of the concrete cylinder.

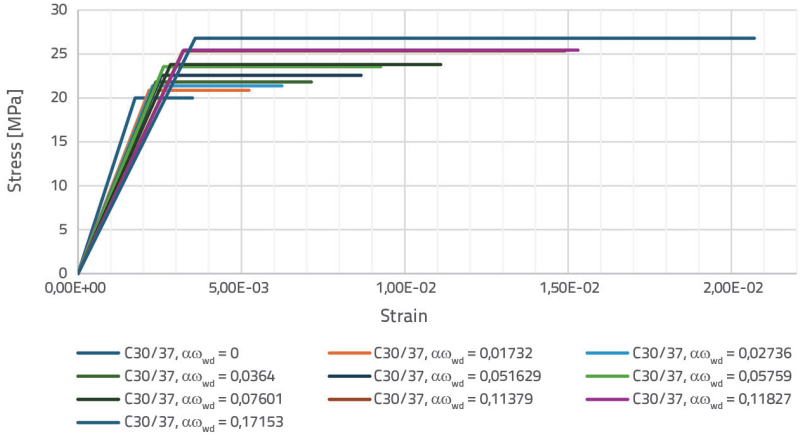

Figure 7. Bilinear design diagrams of confined and unconfined concrete

5.3. Software description

The analysis was performed using the SAP2000 v24.0.0 software with the Section Designer module, employing a general verification method based on equations (7), (8) and (9). The basic working principle is explained using the example in Figure 8, according to [11].
The M – ϕ curve is formed by n calculation points connected by straight lines. Each calculation point is defined by the moment capacity of the cross-section for a given curvature of the section. The number of

calculation points is specified by the user, and each point has a predefined curvature value. Figure 8 shows the cross-section loaded by a known axial force and a defined neutral axis angle. The strain distribution over the cross-section area is defined by the selected curvature value and the position of the neutral axis, i.e., the depth of the compression zone x.

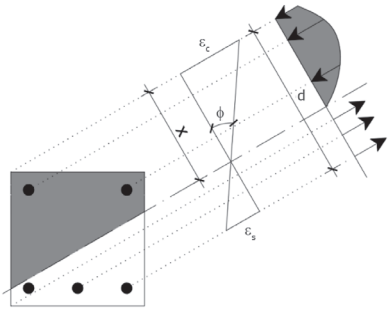

Figure 8. Stress and strain state of the cross-section

Stresses are calculated based on the defined material stress-strain diagrams and the known strains at the points of the section. Since the curvature of the section is predefined for each point on the moment-curvature curve, for each point the depth of the compression zone x is calculated to achieve equilibrium between internal and external forces, using an iterative procedure. After the equilibrium of the axial forces in the cross-section is reached, the moment from the resultant internal forces (compressive forces in reinforcement and concrete and tensile forces in reinforcement) and external forces are calculated. The calculated moment for the defined curvature forms one point of the M – ϕ curve.

5.4. Influence of the level of axial force on the ductility of the reinforced concrete section

5.4.1. "T" Cross section

The influence of the level of axial force on the ductility factor of the T-section was studied on Sections 1 to 7. The sections were loaded with bending moments such that the compression zone was on the flange side. All sections showed high ductility factors in the range 6,36 < μ_ϕ < 13,41 for the normalized axial force ν = 0,20 and a stable, almost linear decrease to values 1,87 < μ_ϕ < 5,68 for the normalized axial force ν = 0,40. The graph in Figure 9 clearly shows the negative impact of axial force on the ductility factor of the section. This can be explained by the larger required length of the compression zone at failure in order to balance the higher axial force. For the same curvature demand as at lower force levels, the most stressed compression fibers require a strain significantly above ε_{cu}. Figure 10 shows the influence of axial force on the depth of the compression zone.

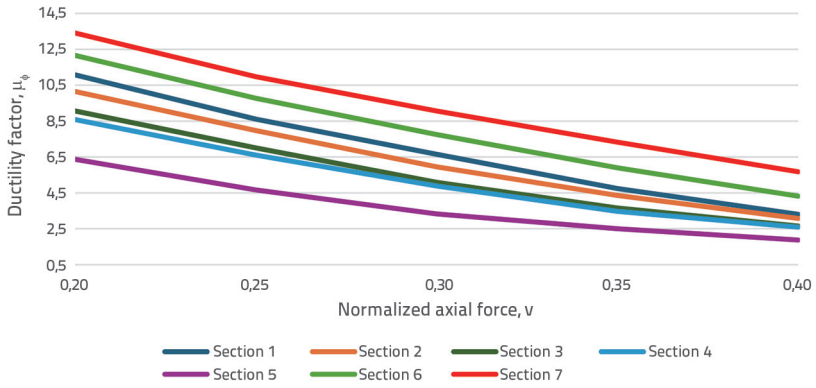

Figure 9. Influence of the normalized axial force level on the ductility factor of Sections 1 to 7

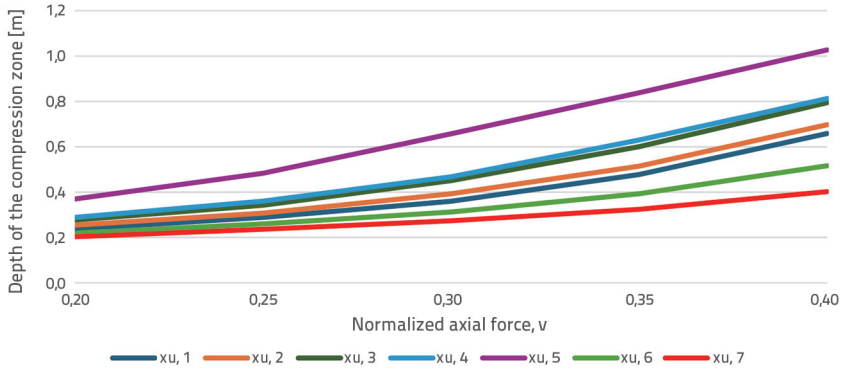

Figure 10. Influence of the normalized axial force level on the depth of the compression zone of Sections 1 to 7

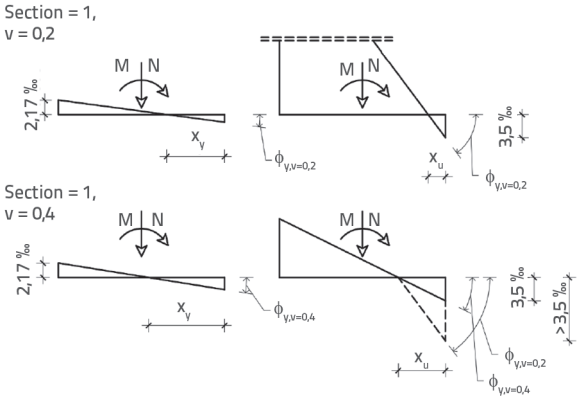

Figure 11. State of strains at tensile reinforcement yielding and failure of Section 1

Figure 11 presents the state of strains at failure and yielding of the tensile reinforcement for Section 1 at axial force levels ν = 0,20 and ν = 0,40. From Figure 11 it can be seen that the ratio of the dephs of the compression zones at ν = 0,20 and ν = 0,40 at tensile reinforcement yielding is greater than at failure. Since the ductility factor of the section relative to curvature is defined as the ratio of the curvature at failure to the curvature at tensile reinforcement yielding, it follows that the reduction in the ductility factor at higher axial force levels is mainly caused by the reduction of curvature at failure. The figure also marks

the curvature $\phi_{u,\nu=0,20}$ with a dashed line, illustrating the increase in required compressive strain of concrete for the larger compression zone depth $x_{u,\nu=0,40}$, which is not achievable in the case of non-confined concrete.

5.4.2. "C" Cross section

The influence of the axial force level on the ductility factor of the "C" section was examined on Sections 21–24. Figure 12 shows the effect of the axial force on the ductility factor of Sections 21, 22, 23, and 24. Similar to the "T" sections, a reduction in ductility with increasing axial force is evident. Unlike the "T" sections, the "C" sections show a faster increase in the depth of the compression zone with increasing axial force, as seen in Figure, Figure 13, this can be attributed to the larger absolute increase in axial force at each step of the analysis. Both types of sections were analyzed for normalized axial force levels from ν = 0,20 to ν = 0,40 in increments of 0,05. The "C" section has a larger cross-sectional area than the "T" section, thus the absolute increase in axial force per step is greater, 1563 kN compared to 813 kN. Since the web widths of both sections are equal, achieving equilibrium at each incremental increase in axial force requires a larger increase in the depth of the compression zone for the "C" section compared to the "T" section.

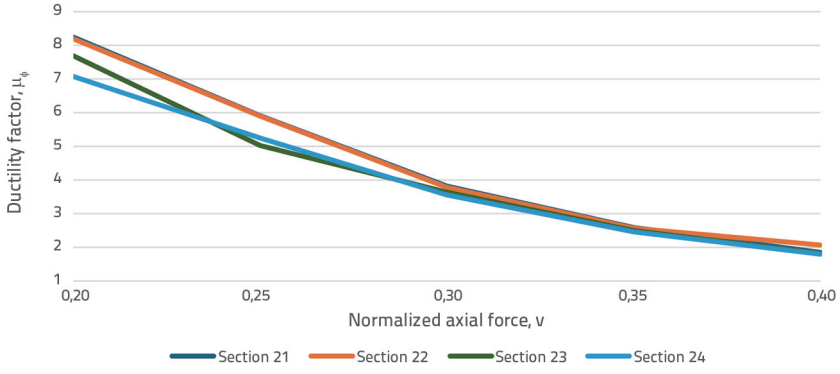

Figure 12. Influence of the normalized axial force level on the ductility factor of Sections 21 to 24

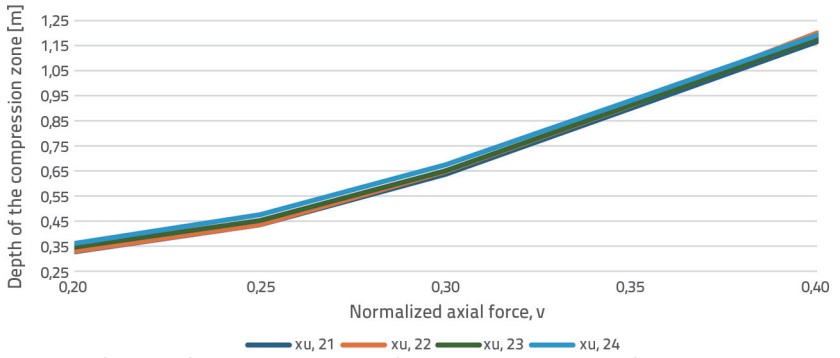

Figure 13. Influence of the normalized axial force level on the depth of the compression zone of Sections 21 to 24

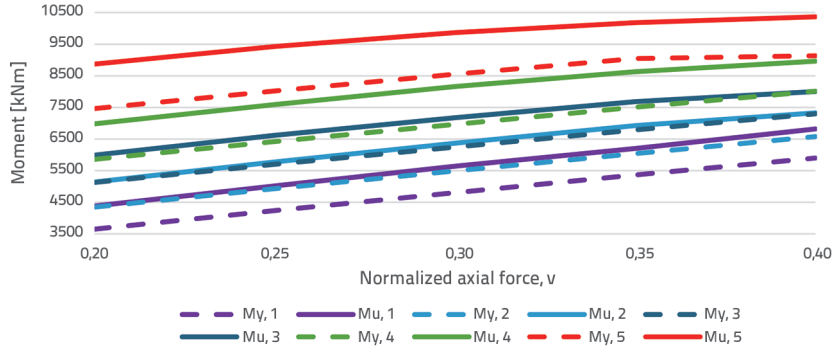

Figure 14. Influence of the normalized axial force level on the moment at tensile reinforcement yielding and the moment capacity of Sections 1 to 5

5.5. Influence of tensile reinforcement on the ductility of the section – "T" Section

The influence of tensile reinforcement on the ductility factor can be seen by comparing Sections 1 to 5 in Figure 9. A decrease in the ductility factor is noticeable with an increase in tensile reinforcement. Increasing the amount of tensile reinforcement raises both the moment at tensile reinforcement yielding and the moment at section failure, as shown in Figure 14, additionally, the depth of the compression zone increases, as shown in Figure 10. The increase in the depth of the compression zone is necessary to balance the greater tensile component of the force couple that forms the moment capacity of the section. The increase in the tensile force component is caused by the increased total amount of tensile reinforcement.

5.6. Influence of compressive reinforcement on the ductility of the section – "T" Section

The beneficial effect of compressive reinforcement on the ductility of the section can be seen by comparing Sections 1, 6, and 7 in Figure 9. The ratio of the elastic moduli of steel and concrete is 200 Gpa / 33 GPa = 6,06. For the same level of strain, reinforcement develops 6,06 times higher stress than concrete and thus contributes more to the compressive capacity of the section. Therefore, increasing the proportion of compressive reinforcement allows the section to achieve the same compressive capacity with a smaller depth of the compression zone compared to a section with less compressive reinforcement. Increasing the amount of compressive reinforcement does not significantly increase the moment at tensile reinforcement yielding or the moment at section failure, as shown in Figure 15.

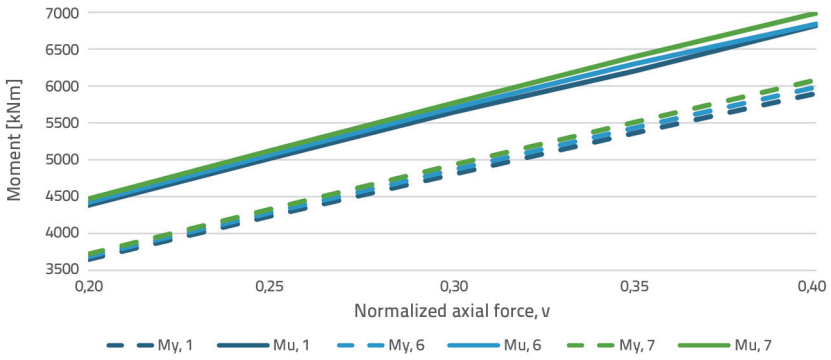

Figure 15. Influence of the normalized axial force level on the moment at tensile reinforcement yielding and the moment capacity of Sections 1, 6, and 7

Figure 10 shows a reduction in the depth of the compression zone in Sections 6 and 7 compared to Section 1 due to a higher amount of compression reinforcement, which results in a lower demand for the compressive strain of the edge fibers and allows for greater curvature of the section at failure. For the permissible strain of unconfined concrete of 3,5 ‰, maximum ductility is achieved with the minimum depth of the compression zone x_{u1}, as shown in Figure 16.

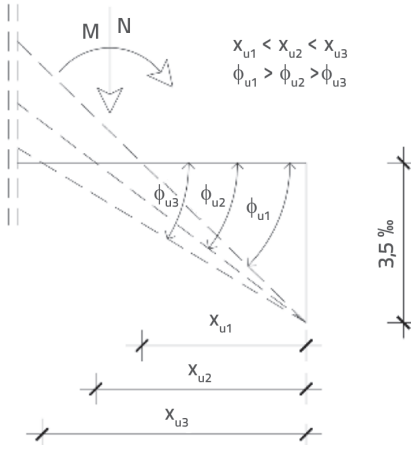

Figure 16. Influence of the compression zone depth on the curvature of the section at failure

5.7. Influence of the variation of compression and tension reinforcement on section ductility – "C" cross section

The influence of varying the compression and tension reinforcement of the section can be observed by comparing Sections 21 to 24 in Figure 12. The "C" shaped sections are symmetrically reinforced. As previously described, an increase in the amount of tensile reinforcement has an adverse effect on the overall ductility factor, in contrast to the favorable effect of compression reinforcement. In Sections 21 to 24, the amount of reinforcement in the flanges and webs was increased equally. The difference in the achieved ductility factor values is more pronounced for lower values of the normalized axial force $\nu \approx 0,2$ and $\nu \approx 0,25$, while for higher levels the values are nearly identical.

Table 2. Analysis results for section 21

Section 21							
ν	$M_{y.21}$ kNm]	$\varphi_{y.21}$	$x_{y.21}$ [cm]	$M_{u.21}$ [kNm]	$\phi_{u.21}$	$x_{u.21}$ [cm]	$\mu_{\phi.21}$
0.20	14025	0.001297	1.0244	16565	0.010690	0.3274	8.242097
0.25	15722	0.001363	1.1062	18284	0.008053	0.4353	5.908291
0.30	17383	0.001427	1.1801	19798	0.005446	0.6372	3.816398
0.35	18992	0.001495	1.2508	20859	0.003872	0.9005	2.589967
0.40	20411	0.001603	1.3473	21533	0.002968	1.1656	1.851528

Table 3. Analysis Results for Section 24

Section 24							
ν	$M_{y.21}$ kNm]	$\varphi_{y.21}$	$x_{y.21}$ [cm]	$M_{u.21}$ [kNm]	$\phi_{u.21}$	$x_{u.21}$ [cm]	$\mu_{\phi.21}$
0.20	21632	0.001347	1.0928	24785	0.009530	0.3606	7.074981
0.25	23307	0.001403	1.1574	26445	0.007359	0.4749	5.245189
0.30	24991	0.001459	1.2171	27922	0.00519	0.6744	3.557231
0.35	26597	0.001526	1.2813	28953	0.003756	0.9313	2.461337
0.40	28025	0.00162	1.36557	29622	0.002913	1.1909	1.798148

Table 4. Comparison of Results for Section 21 and Section 24

ν	$M_{y.21}/M_{y.24}$	$\phi_{y.21}/\phi_{y.24}$	$x_{y.21x}X_{y.24}$	$M_{u.21}/M_{u.24}$	$\phi_{u.21}/\phi_{u.24}$	$x_{u.21}/x_{u.24}$	$\mu_{\phi.21}/\mu_{\phi.24}$
0.20	0.6483450	0.962880	0.937408	0.6683478	1.121721	0.907931	1.164964
0.25	0.6745613	0.971490	0.955763	0.6913972	1.094306	0.916614	1.126421
0.30	0.6955704	0.978067	0.96960	0.7090466	1.049326	0.944840	1.072856
0.35	0.7140655	0.979685	0.976196	0.7204435	1.030884	0.966928	1.052260
0.40	0.7283140	0.989506	0.986619	0.7269259	1.018881	0.978756	1.029686

Tables 2 and 3 present the calculation results for Section 21 and Section 24, while Table 4 provides a comparison of these results:

From the comparison of the analysis results in Table 4, it is evident that the ratio $\phi_{y,21}/\phi_{y,24} \approx 1$ for all levels of normalized axial force, while the ratio $\phi_{u,21}/\phi_{u,24}$ takes values from 1,12 for $\nu = 0{,}20$, to 1,02 for $\nu = 0{,}40$, this indicates that the difference in the achieved ductility factors at lower axial force levels is primarily due to the difference in section curvature at failure. This can be explained by observing the stress distribution diagrams and the depth of the compression zone for Sections 21 and 24 in Figures 17 and 18. Section 21 is reinforced with 4 Ø 16 bars at the intersection of section parts and at the free edges, and with Ø 12/15 cm throughout the remaining section. Section 24 is uniformly reinforced with Ø 25/15 cm, using the same number of bars as Section 21.

At failure, for low values of axial force ν = 0,20 the sections exhibit a shallow compression zone; most of the reinforcement yields, and the external axial force and the tensile force in the reinforcement are balanced by this relatively shallow compressive region. Due to the greater total amount of tensile reinforcement in Section 24, the neutral axis lies deeper at 36,1 cm, compared to 32,7 cm for Section 21. With an increase in the axial force level, the neutral axis shifts downward, the depth of the compression zone increases, the total amount of compressive reinforcement increases, and the amount of tensile reinforcement decreases, that is, as the neutral axis moves, a portion of the tensile-stressed reinforcement transitions to compression. By comparing the $x_{u,21}/x_{u,24}$ ratio in Table 4 a convergence of $x_{u,21}$ and $x_{u,24}$ values can be observed with increasing axial force. As a result of this convergence in neutral axis depths and given the same maximum allowable concrete strain of 3,5 ‰, the ductility factors of the sections tend to converge with increasing axial force.

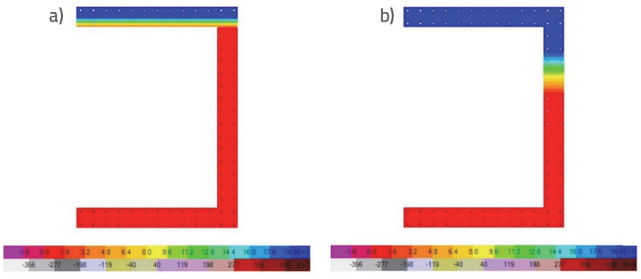

Figure 17. Stress state representation, a) Section 21 ν = 0,2, b) Section 21 ν = 0,4

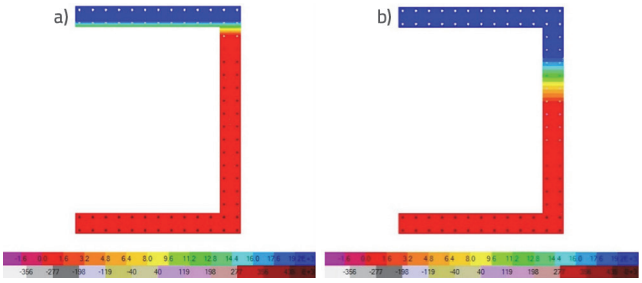

Figure 18. Stress state representation, a) Section 24 ν = 0,2, b) Section 24 ν = 0,4

5.8. Influence of concrete confinement on the moment – curvature diagrams of cross sections

The effects of partial confinement of the concrete web in the "T" sections at Sections 12 to 15, and confinement of the concrete flanges in the "C" sections at Sections 31 to 34.

5.8.1. "T" Section

Sections 11, 12, 13, 14, and 15 are considered. Section 11 corresponds to Section 4 analyzed for the opposite direction of bending moment compared to Section 4. Sections 12, 13, 14, and 15 are sections with a confined part of the web; they have the same longitudinal reinforcement, a concrete cover of c = 2,5 cm and the dimensions of the confined web part. The dimensions of the confined concrete core are 39,5 cm × 19 cm. The chosen confinement method consists of a single closed stirrup, longitudinal "C" hooks, and three transverse "C" hooks. Section 12 is confined with reinforcement Ø8/15 cm, Section 13 with reinforcement Ø10/15 cm, Section 14 with reinforcement Ø10/10 cm and Section 15 with Ø10/7,5 cm. The corresponding confinement effectiveness coefficients α and mechanical reinforcement coefficients ω_{wd} for the confined reinforcement were calculated. The part of the section within the confined concrete core is defined by the characteristics of the confined concrete shown in Figure 7, the following is a tabular presentation of the sections, corresponding confinement reinforcement, and characteristics of the confined concrete.

Figure 19 shows the graph of the ductility factor dependence on the normalized axial force for the analyzed sections. With the increasing curvature of Section 11, and due to the absence of flange confinement and a larger area in the compression zone,

Table 5. Data on confined sections 12, 13, 14, and 15

Section	Confinement reinforcement [cm]	$\alpha\omega_{wd}$	Characteristics of confined concrete [MPa]
Section 12	Ø8/15	$\alpha\omega_{wd}$ = 0.03640	$\varepsilon_{c3.c}$ = 0.0023806; $\varepsilon_{cu3.c}$ = 0.007140 $f_{cd.c}$ = 23.82
Section 13	Ø10/15	$\alpha\omega_{wd}$ = 0.05759	$\varepsilon_{c3.c}$ = 0.0026174; $\varepsilon_{cu3.c}$ = 0.009259 $f_{cd.c}$ = 23.55
Section 14	Ø10/10	$\alpha\omega_{wd}$ = 0.11379	$\varepsilon_{c3.c}$ = 0.0032118; $\varepsilon_{cu3.c}$ = 0.014879 $f_{cd.c}$ = 25.35
Section 15	Ø10/7.5	$\alpha\omega_{wd}$ = 0.17153	$\varepsilon_{c3.c}$ = 0.003588; $\varepsilon_{cu3.c}$ = 0.0206530 $f_{cd.c}$ = 26.79

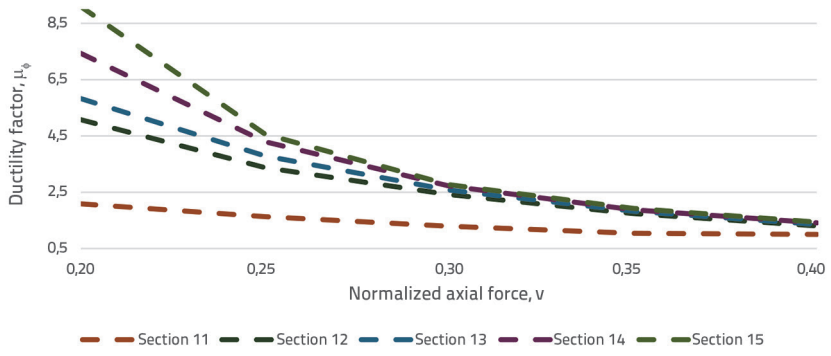

Figure 19. Influence of the normalized axial force level on the ductility factor of Sections 11 to 15

there is a rapid increase in the depth of the compression zone and exhaustion of the compressive strains of the unconfined concrete. The achieved ductility factor values for Section 11 are low, and for normalized axial force levels $\nu \geq 0,35$ the ductility of the section tends to 1. By applying confinement to part of the web in Sections 12–15, higher ductility factor values are achieved, especially for low levels of axial force. For higher axial force levels, the beneficial effect of concrete confinement decreases due to the exceeding of the strain of the unconfined concrete in the web adjacent to the confined concrete, which results in its exclusion from the section's load-bearing capacity, an increase in the depth of the compression zone, and utilization of the maximum strain of the confined concrete.

A representation of the stress state of Section 15 at failure for levels $\nu = 0,20$ and $\nu = 0,25$ is given.

For levels of $\nu \geq 0,25$ due to the decrease in the section's moment capacity with increasing curvature, the ductility of the section with respect to curvature was calculated at the curvature corresponding to the yielding of the tensile reinforcement and at the curvature corresponding to $0,85M_{max}$. The decrease in moment capacity is caused by the exceeding of the compressive strains of the unconfined concrete and its exclusion from the

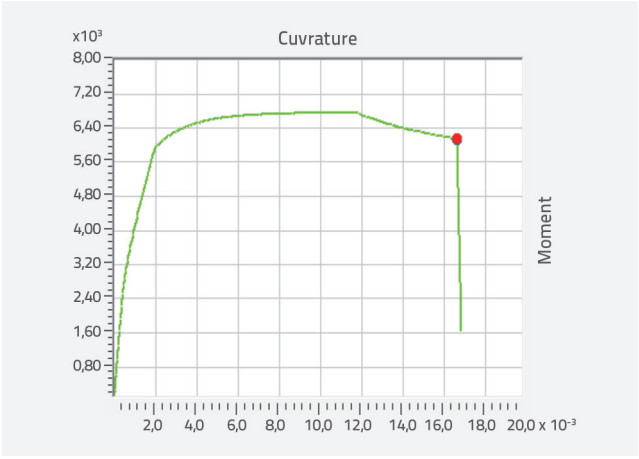

Figure 20. M – ϕ diagram for Section 15 at $\nu = 0,20$

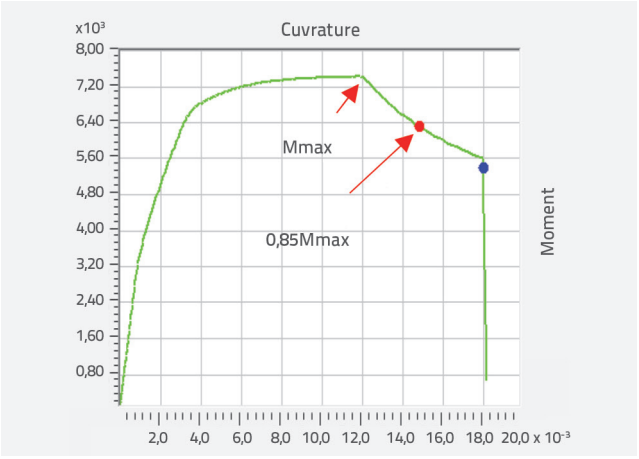

Figure 22. M – ϕ diagram of Section 15 for $\nu = 0,25$

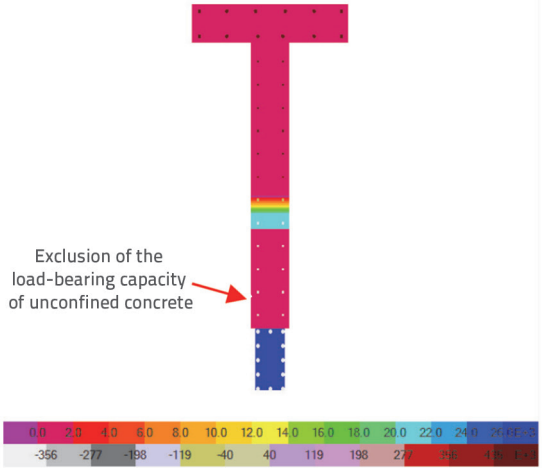

Figure 21. Stress state at failure of Section 15 for $\nu = 0,20$

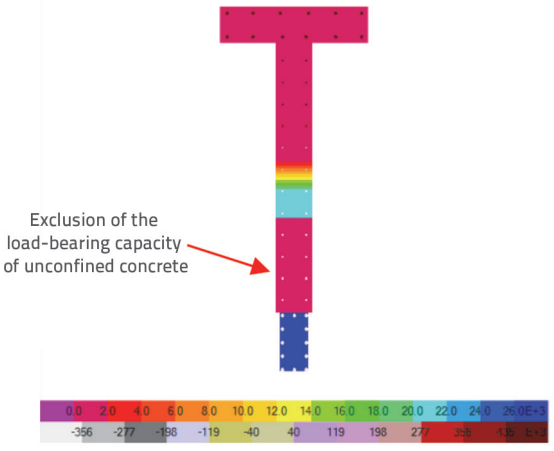

Figure 23. Stress state at failure of Section 15 for $\nu = 0,25$

Table 6. Data on Confined Sections 31, 32, 33, and 34

Section	Confinement reinforcement [cm]	$\alpha\omega_{wd}$	Characteristics of confined concrete [MPa]
Section 31	Ø8/15	$\alpha\omega_{wd}$ = 0.01732	$\varepsilon_{c3.c}$ = 0.0021769; $\varepsilon_{cu3.c}$ = 0.005232; $f_{cd.c}$ = 20.87
Section 32	Ø10/15	$\alpha\omega_{wd}$ = 0.02736	$\varepsilon_{c3.c}$ = 0.002283; $\varepsilon_{cu3.c}$ = 0.006236; $f_{cd.c}$ = 21.37
Section 33	Ø10/10	$\alpha\omega_{wd}$ = 0.05163	$\varepsilon_{c3.c}$ = 0.0025496; $\varepsilon_{cu3.c}$ = 0.008663; $f_{cd.c}$ = 22.58
Section 34	Ø10/7.5	$\alpha\omega_{wd}$ = 0.07601	$\varepsilon_{c3.c}$ = 0.0028323; $\varepsilon\varepsilon_{cu3.c}$ = 0.011100; $f_{cd.c}$ = 23.8

load-bearing capacity, which is evident at the failure point of the M – ϕ diagram at M_{max}.

5.8.2. "C" Section

Sections 24, 31, 32, 33, and 34 are considered. The sections have the same longitudinal reinforcement, a concrete cover of 2,5 cm and the same area of confined concrete. The selected confinement method involves tying the longitudinal bars with "C" hooks and a closed stirrup along the perimeter of the flange. The corresponding confinement effectiveness coefficients α and mechanical reinforcement coefficients ω_{wd} were calculated. Section 31 is confined with Ø8/15 cm reinforcement, Section 32 with Ø10/15 cm, Section 33 with Ø10/10 cm and Section 34 with Ø10/7,5 cm. The part of the section within the confined concrete core is defined by the properties of confined concrete as shown in Figure 7. Table 6 presents the selected confinement reinforcement and the characteristics of the confined concrete for Sections 31–34:

A graph showing the dependence of the ductility factor on the normalized axial force is presented:

From the graph in Figure 24 a favorable effect of flange concrete confinement is noticeable, particularly at lower values of normalized axial force ν = 0,20 and ν = 0,25, At higher levels of axial load, the beneficial effect of concrete confinement decreases due to the exceeding of the strain of the unconfined web concrete adjacent to the confined flange, similarly to the behavior observed in the confined "T" section. A representation of the stress state for Section 34 at failure is given for axial force levels $\nu \geq$ 0,20 and $\nu \geq$ 0,25.

From the graph in Figure 24 a slightly lower ductility of Section 31 compared to the reference Section 24 is observed. The compression flange of Section 31 is defined by the area of confined concrete in order to simulate the spalling of the concrete cover when the allowable compressive strains of unconfined concrete are exceeded. Section 31 has the lowest product $\alpha\omega_{wd}$ = 0,01732 and the properties of the confined concrete differ only slightly from those of

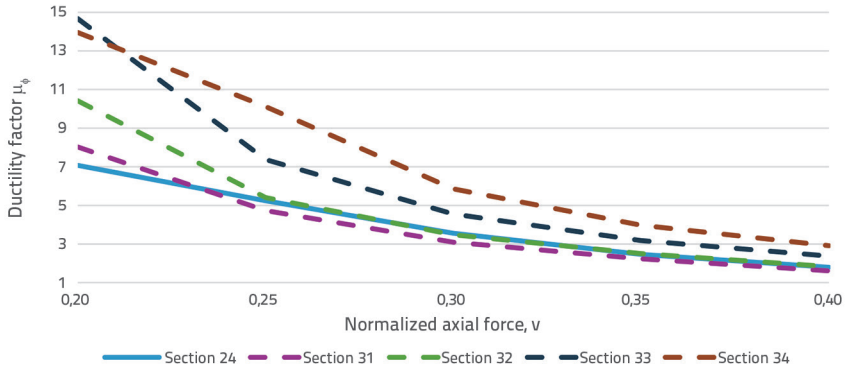

Figure 24. Influence of the normalized axial force level on the ductility factor of Sections 24, 31 to 34

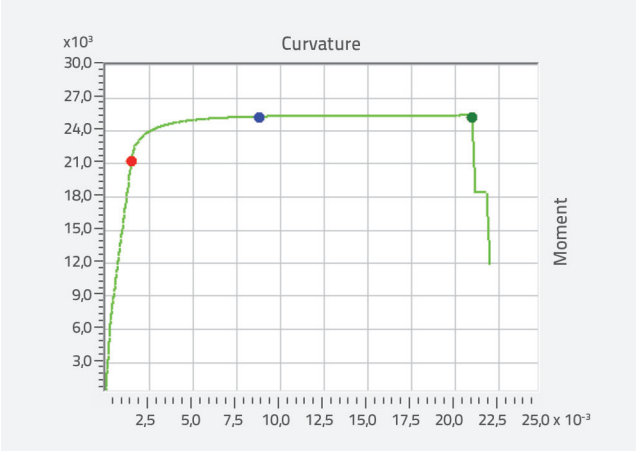

Figure 25. M – ϕ diagram of Section 34 for ν = 0,20

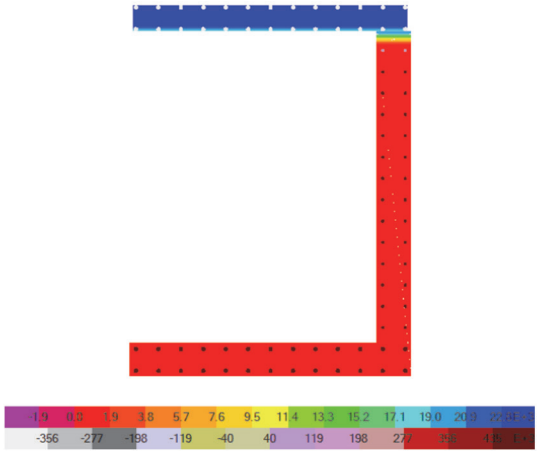

Figure 26. Stress state at failure of Section 34 for ν = 0,20

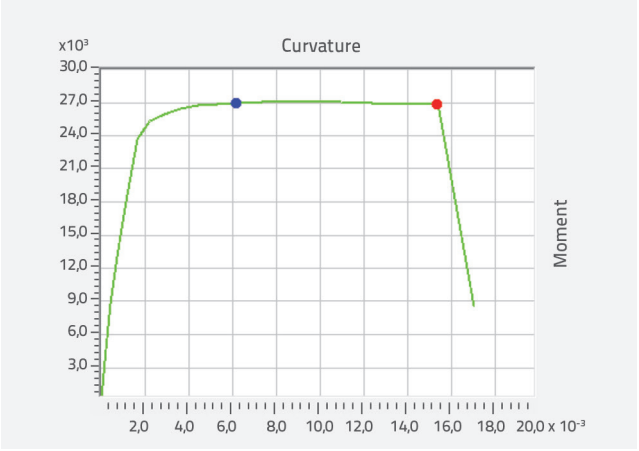

Figure 27. M – ϕ diagram of Section 34 for ν = 0,25

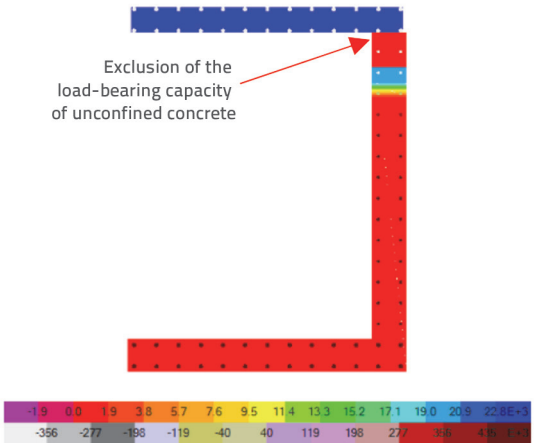

Figure 28. Stress State at failure of Section 34 for ν = 0,25

unconfined concrete. The beneficial effects of mild confinement in the reduced flange area are not sufficient to offset the impact of the reduced section area caused by the spalling of the concrete cover.

5.9. Analysis of results

According to HRN EN 1998-1 [6] in critical wall regions it is necessary to ensure a ductility factor μ_φ with respect to curvature that is at least equal to the value calculated from equation (4) with the basic behavior factor q_0 which in those expressions is replaced by the product of q_0 and the maximum value of the ratio M_{Ed}/M_{Rd} at the base of the wall for the seismic design situation, where M_{Ed} is the design bending moment from the analysis, and M_{Rd} is the design bending resistance.

Assuming that the analyzed sections constitute the load-bearing structure of a building designed adopting a behavior factor of 3,0 for ductile unconfined walls and achieving a ratio M_{Ed}/M_{Rd} = 0,9, for a building with period $T_1 > T_c$, according to equation (4) the required ductility factor μ_ϕ is 6,6. An overview of all analyzed sections is given:

In Figure 29 the required ductility factor level μ_ϕ = 6,6, is marked. It is visible that for low levels of normalized axial force ν = 0,20 almost all sections except Sections 11, 12, 13, and 5 meet the ductility requirement. For the normalized axial force level ν = 0,40 none of the analyzed sections satisfy the ductility requirement.

6. Conclusion

This paper describes the ductility property of sections as a fundamental characteristic of elements that make up the load-

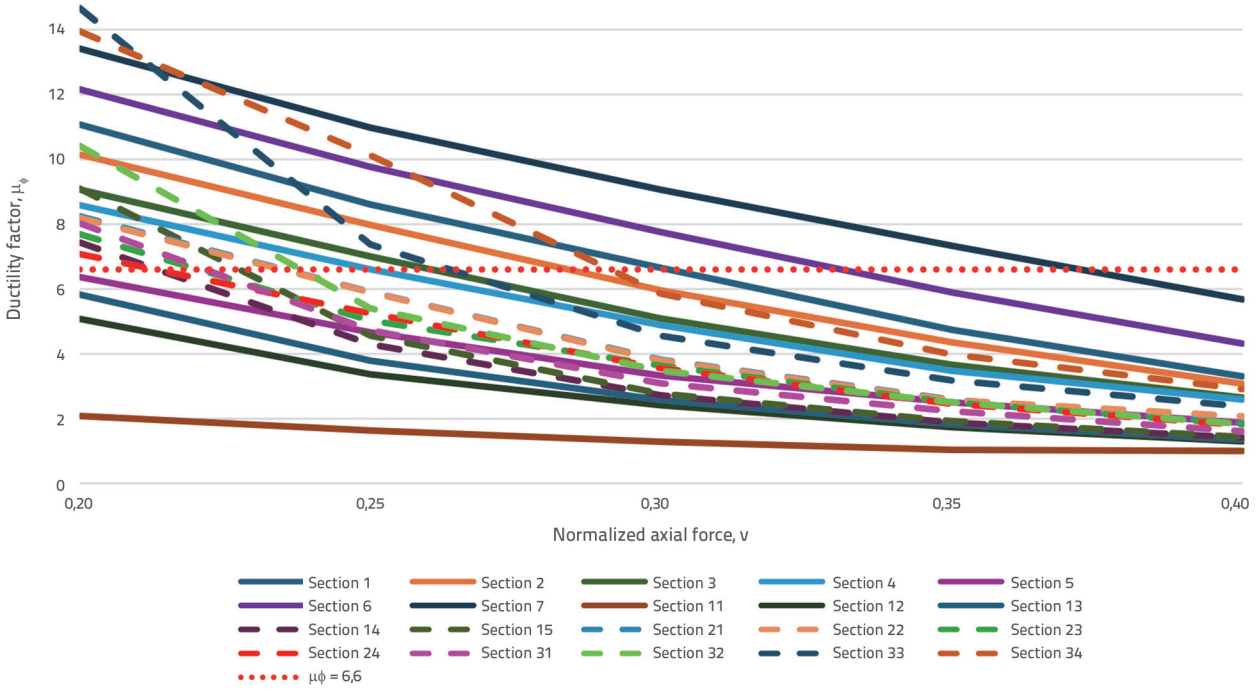

Figure 29. Influence of the normalized axial force level on the ductility factor of the sections

bearing structure resistant to seismic action. Sections of "T" and "C" shapes were analyzed for normalized axial force levels ν = 0,20, ν = 0,25, ν = 0,30, ν = 0,35 and ν = 0,40 varying the amount and arrangement of reinforcement and the degree of confinement of parts of the sections.

The main factors controlling the available ductility of the sections were found to be the maximum allowable compressive strain of the concrete and the depth of the compression zone. It was shown that the ductility of the sections significantly decreases with increasing axial force, primarily due to the reduction of the section curvature at failure. Increasing the tensile reinforcement of the section also reduces the ductility factor, while increasing the compression reinforcement has a favorable effect. Increasing the amount of compression and tensile reinforcement in the "C" section influences the ductility factor only at lower levels of axial force. For "T" shaped sections, the available ductility varies significantly depending on the considered direction of the section's moment capacity. Confinement of parts of the section increases the available ductility. In cases of insufficient confinement length of the flange, failure of the unconfined part of the section occurs, leading to accelerated growth of the compression zone depth and section failure. If the analyzed sections formed the structural system of the building, at higher levels of axial force they would not satisfy the expected required ductility factor μ_ϕ = 6,6. The ductility of the sections can be increased by enlarging the dimensions of the compression part of the section or by increasing the concrete grade, which reduces the depth of the compression zone, or by confining the concrete to increase the maximum compressive strain of the concrete. At high levels of axial stress, it is reasonable to increase the wall section size or concrete grade to reduce the demand for confinement, simplify reinforcement details, and facilitate concrete placement. For sections without a flange or with a relatively larger compression area, such as Sections 12 to 15, small values of the ductility coefficient can be expected, and special attention should be paid to their design.

Considering the complexity and lack of expressions describing the behavior of walls with composite cross-sections, further research should focus on the analysis of walls at the element level, as well as the influence of shear forces, torsional moments, tensile reinforcement pull-out, diagonal bending, and deviations from the assumption of plane cross-sections on the values of ductility coefficients. Including these effects in analytical and numerical models would result in more accurate predictions of the actual behavior of walls with composite cross-sections.

REFERENCES

[1] Kuk, K., Ivančić, I., Sović, I., Mustać, M., Fiket, T., Šariri, K.: Priručnik za integraciju seizmoloških podataka: Seizmološka služba pri Geofizičkom odsjeku Prirodoslovno-matematičkog fakulteta Sveučilišta u Zagrebu: Zagreb: 2023: p. 35.

[2] Capannelli, E., Katić, K., Vojković, M., Bogaerts, V.R., Stanton-Geddes, Z.: CROATIA EARTHQUAKE Rapid Damage and Needs Assessment 2020, Vlada Republike Hrvatske, Zagreb, 2020: p. 14.

[3] Penelis, G., Penelis, G.: Concrete Buildings in Seismic Regions, Second edition: Taylor & Francis: Boca Raton, FL, SAD, 2019, pp. 128-164 .

[4] Park, R., Paulay, T.: Reinforced Concrete Structures: John Wiley & Sons, Inc., New York, 1975, pp. 547-549 .

[5] Fardis, M.N.: Seismic Design, Assessment and Retrofitting of Concrete Buildings, Springer, Dordrecht, Heidelberg, London, New York, 2009, pp. 436 – 462.

[6] Eurokod 8: Projektiranje potresne otpornosti konstrukcije -1. dio:Opća pravila, potresna djelovanja i pravila za zgrade, CEN, Brussels, Belgija, 2004, pp. 69 – 88.

[7] Eurokod 2: Projektiranje betonskih konstrukcija-Dio 1-1: Opća pravila i pravila za zgrade, CEN, Brussels, Belgija, 2013, pp. 40-41.

[8] Eurokod 8: Projektiranje potresne otpomosti konstrukcija-3. dio: Ocjenjivanje i obnova zgrada, CEN, Brussels, Belgija, 2011, pp. 33-34.

[9] Konstantinidis, A.: EARTHQUAKE RESISTANT BUILDINGS from reinforced concrete: pi-SYSTEMS INTERNATIONAL S.A., Grčka, 2008.

[10] Kišiček, T., Sorić, Z.: Bending moment-curvature diagram for reinforced-concrete girders, Građevinar, 55 (2003) 4, pp. 207-215.

[11] Structures and Computers: Section Designer Manual: Structures and Computers, Berkeley, California, SAD, 2000, pp. 110-118.

[12] Kuk, V., Prelogović, E., Sović, I., Kuk, K., Šariri, K.: Seizmološke i seizmotektonske značajke šireg zagrebačkog područja, Građevinar, 52 (2000) 11, pp. 647-653.

[13] Mrak, P., Grandić, D., Meštrović, D.: Armiranobetonski zidovi u potresnim područjima, Građevinar, 62 (2010) 6, pp. 517-527.

[14] Šavor Novak, M., Uroš, M., Atalić, J., Herak, M., Demšić, M., Baniček, M., Lazarević, D., Bijelić, N., Crnogorac, M., Todorić, M.: Zagreb earthquake of 22 March 2020 – Preliminary report on seismologic aspects and damage to buildings, Gradjevinar, 72 (2020) 10, pp. 843-867, https://doi.org/10.14256/JCE.2966.2020

[15] Radnić, J., Grgić, N., Buzov, A., Banović, I., Zulim, M. S., Baloević, G., Sunara, M.: Mw 6.4 Petrinja earthquake in Croatia: Main earthquake parameters, impact on buildings and recommendation for their structural strengthening, Građevinar, 73 (2021) 11, pp. 1109-1128, https://doi.org/10.14256/JCE.3243.2021

[16] Simović, V.: Potresi na zagrebačkom području, Građevinar, 52 (2000) 11, pp. 637-645.